ANALYSIS OF X-BAND POLARIMETRIC SAR DATA FOR THE DERIVATION OF THE SURFACE ROUGHNESS OVER BARE AGRICULTURAL FIELDS

Nicolas Baghdadi[1], Noha Holah[1], Pascale Dubois-Fernandez[2], Laurent Prévot[3], Steven Hosford[1], André Chanzy[3], Xavier Dupuis[2], Mehrez Zribi[4]

[1] French Geological Survey (BRGM), 3 avenue C. Guillemin, B.P. 6009, 45060 Orléans cedex 2, France, n.baghdadi@brgm.fr
[2] ONERA, Base Aérienne 701, 13661 Salon AIR cedex, France
[3] INRA, Unité Climat Sol et Environnement, Domaine St Paul, 84914 Avignon cedex 9, France
[4] CETP/CNRS, 10/12, avenue de l'Europe, 78140 Velizy, France

Commission PS, WG I/3

KEY WORDS: Remote Sensing, SAR, Soil, Land Cover, Land Use, Agriculture

ABSTRACT:

We investigated the potential of fully polarimetric data in X-band to discriminate the principal surface types present in a study site near Avignon in France: bare soils, agricultural fields, orchards (various fruits), forest, buildings, residential houses, and roads. Decomposition and analysis techniques have been applied to a data set acquired by the ONERA airborne RAMSES SAR. The discrimination potential of various polarimetric parameters (entropy, $\overline{\alpha}$-angle, anisotropy) have been discussed. Results show that X-band provides some discrimination capability. The polarimetric parameters, *entropy* and $\overline{\alpha}$-*angle*, show clearly that these classes' signatures are grouped in five clusters corresponding to physical scattering characteristics. The introduction of the parameter *anisotropy* does not improve our ability to distinguish between different classes whose clusters are in the same entropy/$\overline{\alpha}$-angle zone. We observe a very weak correlation between the signal radar and the surface roughness over bare soils.

1. INTRODUCTION

A polarimetric SAR system measures the complete complex scattering matrix [S] of a medium with quad polarizations. This matrix is made up of the complex scattering coefficients S_{pq}, where p is the transmitting polarization and q the receiving polarization (p , q = H (Horizontal) or V (Vertical)). The polarimetric information of a target can be represented by a scattering coherency matrix [T] which can be calculated directly from the complex scattering vector as follows (Cloude and Pottier, 1996):

$$\langle [T] \rangle = \langle k_p \cdot k_p^{*T} \rangle$$

with

$$k_p = \frac{1}{\sqrt{2}} \begin{pmatrix} S_{HH} + S_{VV} \\ S_{HH} - S_{VV} \\ 2S_{HV} \end{pmatrix}$$

where k_p is the target vector of [S], the superscripts *, ^{T} and <.> denote respectively the complex conjugate, the matrix transpose, and spatial averaging over a group of neighbouring pixels using a sliding window. Coherency matrices are frequently processed for speckle reduction by averaging the pixels in a 5x5 window.

Landcover classification using a fully polarimetric SAR image is one of the most important applications of radar polarimetry in remote sensing. Over the last few years, polarimetric data has been successfully used for various applications for example: the classification of sea ice, the derivation of land surface parameters (surface roughness and soil moisture), and the classification of trees according to age in a forest environment (Scheuchl et al., 2001; Hajnsek et al., 1999; Ferro-Famil and Pottier, 2001; etc.). However, the majority of these studies have been conducted using polarimetric data in P, L and C bands. In this paper, we have applied polarimetric processing techniques to SAR data in order to evaluate the potential of X-band. The overall objective of this study is to evaluate fully polarimetric information by analysing the separability between the different landcover classes present on the study site and thus derive the parameters that are of most use in their classification.

2. POLARIMETRIC SAR DATA DECOMPOSITION

Cloude and Pottier (1996) have proposed a polarimetric decomposition theorem based on the eigenvalue/eigenvector decomposition of the coherency matrix into elementary mechanisms (i.e. single, double and volume scattering) in order to identify the global mean scattering mechanism. The matrix [T] can be decomposed into its eigenvector basis using the following equation:

$$\langle [T] \rangle = \sum_{i=1}^{3} \lambda_i V_i V_i^{*T}$$

where λ_i are the three eigenvalues of <[T]>, real and non-negative $\lambda_1 \geq \lambda_2 \geq \lambda_3 \geq 0$. V_i are the related orthogonal unitary eigenvectors. The eigenvectors are parameterised using 4 angular variables leading to an interpretation of the scattering phenomenon:

$$V_i = \left[\cos\alpha_i, \sin\alpha_i \cos\beta_i \, e^{j\delta_i}, \sin\alpha_i \sin\beta_i \, e^{j\gamma_i} \right]^T$$

where α_i, β_i, δ_i, and γ_i represent a set of four independent parameters characterising the fully polarised backscattered field.

Using eigenvectors and eigenvalues, three main parameters are used to characterise the results of this decomposition: entropy (H), $\overline{\alpha}$-angle, and anisotropy (A). The entropy H is defined from the logarithmic sum of eigenvalues of <[T]> and represents the random behaviour of the global scattering:

$$H = -\sum_{i=1}^{3} P_i \cdot \log_3(P_i) \quad , \quad 0 \leq H \leq 1$$

where P_i are the normalised eigenvalues :

$$P_i = \frac{\lambda_i}{\sum_{j=1}^{3} \lambda_j}$$

The entropy H is a measure of randomness of scattering mechanisms. Low entropy ($H\sim0$) indicates a single scattering mechanism (isotropic scattering) while high entropy ($H\sim1$) indicates a totally random mixture of scattering mechanisms with equal probability and hence a depolarizing target.

The parameter $\overline{\alpha}$ represents the mean dominant scattering mechanism and is calculated from the eigenvectors and eigenvalues of $<[T]>$:

$$\overline{\alpha} = \sum_{i=1}^{3} \alpha_i P_i$$

where α_i are the scattering mechanisms represented by the three eigenvectors. $\overline{\alpha}=0°$ indicates a surface scattering, $\overline{\alpha}=45°$ a volume scattering, and $\overline{\alpha}=90°$ a double bounce scattering from metallic surfaces (dihedral scatter).

The anisotropy A indicates the distribution of the two less significant eigenvalues:

$$A = \frac{\lambda_2 - \lambda_3}{\lambda_2 + \lambda_3} \quad , \quad 0 \leq A \leq 1$$

where λ_2 and λ_3 are the two lowest eigenvalues.

It becomes 0 if both scattering mechanisms are of an equal proportion while values of A>0 indicates increasing amounts of anisotropic scattering.

3. DATA SET

Fully polarimetric X-band radar data were acquired by the airborne RAMSES SAR of the French Aerospace Research Center (ONERA) on March 20, 2002 over a study site near Avignon (south of France). A single swath of about 1.8 km width and 5.2 km long was acquired with incidence angles ranging from 13° to 36°. Image quality was excellent except for the range between 13° and 16° where blurring and banding were apparent. The SAR data were processed and calibrated at ONERA. The slant-range resolution and the azimuth resolution were 0.66 and 0.64 m, respectively. A segment of the SAR image used in this study is shown in Figure 1, which shows the polarization colour composite image. HH is displayed as red, HV as green, and VV as blue.

The study site consist mainly of agricultural landscape. It includes agricultural areas, forest stands, houses, buildings, and roads. The agricultural areas are composed mainly of bare soils and wheat fields. But include orchards of various fruit trees, among them peach, pear and apricot. The forest area present in the image is mainly covered with pine and herbaceous. The buildings can be considered to be of three distinct types: houses, low building (1 - 2 floors) and high building (3 floors or more). In general, the buildings are characterised by their flat roofs (mostly composed of gravel or tar). During the SAR survey, four trihedrals and one dihedral were deployed.

During the SAR survey, ground photographs and field surveys were conducted in order to facilitate the identification of different surface types and to measure the characteristics of the agricultural areas. The ground truth measurements were carried out on wheat fields and on bare soils. Measurements of soil roughness were carried out on five bare soil fields (R1 to R5) using 2-m long needle profilometers of with 1-cm sampling intervals. Ten roughness profiles were established for each training field. From these measurements, the standard deviation of surface height (rms) were calculated. The soil moisture at field scale was assumed to be equal to the mean value estimated from 15 samples (per field) collected from the top 1 cm of soil using the gravimetric method. The surface roughness (rms) and soil moisture (mv) fall within the ranges: 0.80 cm<rms<2.40 cm and 8.6%<mv<22.2% (Table 1). At the time of the image acquisition, the fields R1 to R4 were freshly tilled whereas R5 had been tilled several months before. The soil is composed of about 53.0% loam, 31.6% clay and 15.4% sand.

Field ID	Incidence angle (°)	Soil moisture 0-1 cm (%)	rms surface height (cm)	Correlation length (cm)
R1	26.1	15.7	2.40±0.20	5.51±1.65
R2	26.3	20.0	1.64±0.20	4.43±1.21
R3	26.5	21.0	1.28±0.15	3.34±0.64
R4	26.6	22.2	0.85±0.15	3.04±0.98
R5	31.7	8.6	0.80±0.22	6.42±1.99

Table 1. Ground measurements study site Avignon.

4. DATA ANALYSIS

4.1 Image Interpretation

A photo-interpretation of the composite image presented in Figure 1 shows that the difference in backscatter is pronounced between certain surface types. The bright signature is attributed to multiple bounce scattering (presence of buildings, houses, dihedral and trihedrals). Roads, on the other hand, are very smooth surfaces, and thus appear in a very dark tone on the image. Forests, wheat and fruit trees would seem to have very similar signatures on the imagery. Similarly, it is impossible to distinguish the various roughness states of the areas of bare soil which have a rms surface height between 0.85 and 2.4 cm (fields R1, R2, R3 and R4).
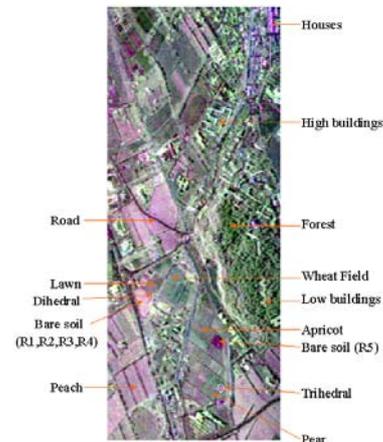
Figure 1. Segment of the X-band RAMSES image. HH, HV and VV are respectively coded in red, green and blue. The incidence angles range from 25° on the left side of the image to 36° at the right side.

4.2 Signature Study

Image analysis was carried out to study the behaviour of the principal surface types on the study site (bare soil fields with varying surface roughness, wheat fields, orchards, forest areas, buildings, houses and roads) and to investigate the polarimetric parameters extracted from SAR data in order to discriminate the observed classes. The parameters chosen correspond to parameters frequently used in the literature: backscattering coefficients, copolarization and depolarization ratios, magnitude of the correlation coefficients, entropy, $\overline{\alpha}$ -angle, and anisotropy. For each surface type, several training sites based on field observations were selected. Statistical analysis of various parameters for various targets are shown in Figure 2. Each point plotted represents the parameter mean value for a given training site (e.g. a field). This is calculated by averaging the values of all the pixels from the site.

Results show that the backscattering coefficients are ineffective in discriminating the different classes. We observe a poor separation between the areas of vegetation (forest, wheat, …) for all polarizations, a good separation between different building types especially in HV polarization, and a moderate separation between bare soils and the other natural classes in HH and VV polarizations. Roads can be easily differentiated from the surface types using the HV polarization.
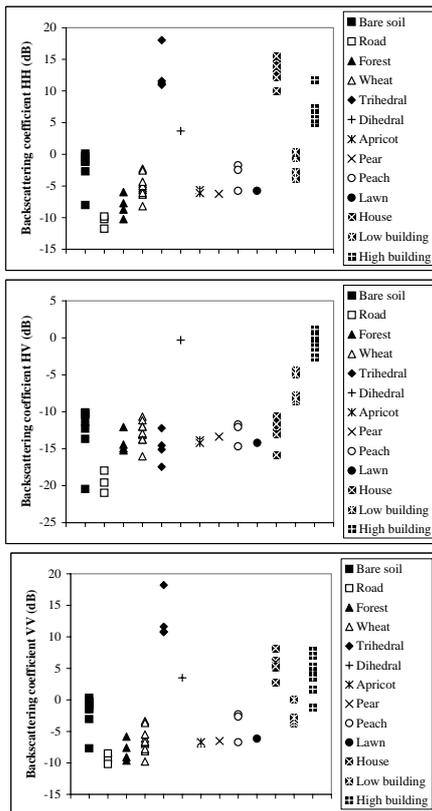
Figure 2 . Behaviour of different parameters of the radar signal calculated from X-band polarimetric SAR data in function of various cover types.

The copolarization and depolarization ratios show poor separability between classes. Only the house class can be extracted without ambiguity using depolarization ratios. However, the polarization ratios HV/HH and VV/HH show good discrimination between forest and wheat. Bare soils and roads are clearly distinguishable from the other classes in using the ratio HV/VV but are not themselves separable.

Concerning the degree of coherence between different polarizations, results show that the correlation between copolar and cross polar is low for natural areas and the potential for discrimination between different classes is poor. The correlation between HH and VV is high for all classes except for low buildings and forest where the correlation is medium. This correlation parameter allows a good separability between bare soils and the other classes.

Concerning the interpretation of polarimetric parameters (entropy, $\overline{\alpha}$ -angle and anisotropy), Cloude and Pottier (1997) have proposed a division of the entropy and $\overline{\alpha}$ -angle plane into eight zones of different scattering behaviour, in order to separate the data into basic scattering mechanisms. Each of the eight zones corresponds to very specific physical scattering characteristics:

> Zone 1: High entropy multiple scattering
> Zone 2: High entropy volume scattering
> Zone 3: Medium entropy multiple scattering
> Zone 4: Medium entropy volume scattering
> Zone 5: Medium entropy surface scattering
> Zone 6: Low entropy multiple scattering
> Zone 7: Low entropy volume scattering
> Zone 8: Low entropy surface scattering

Figure 3a shows the distribution of airborne RAMSES data in the H/$\overline{\alpha}$ plane with the valid region for coherency matrix data shown with a dotted line. The distribution of H/$\overline{\alpha}$ values shows that the distribution is concentrated at low to medium entropy. Also, we observe overlapping of the polarimetric parameters within H/$\overline{\alpha}$ plane for different classes. The analysis of entropy and $\overline{\alpha}$ -angle enable us to discriminate five principal groups of clusters:

- Houses and dihedral: low entropy multiple scattering (double bounce scattering) and high values for the $\overline{\alpha}$ -angle (zone 6).
- Trihedrals: low entropy surface scattering and low values for the $\overline{\alpha}$ -angle (zone 8).
- High building: medium entropy multiple scattering and high values for $\overline{\alpha}$ (zone 3).
- Low building and forest: medium entropy volume scattering and medium values for $\overline{\alpha}$ (zone 4). It is impossible to distinguish between these two classes in the H/$\overline{\alpha}$ plane.
- Wheat fields, lawns, orchards, bare soils and roads: medium entropy and low values for $\overline{\alpha}$ (zone 5). For wheat fields, lawns and orchards, surface scattering is the dominant process at X-band, however a second less significant scattering process resulting from the interaction with the vegetation layer (volume scattering) is present. The medium entropy observed for wheat, for example, is most probably due to penetration of the radar wave through the vegetation canopy. This penetration is however weak in X-band. Over roads and bare soils mainly surface scattering appear.

In addition, targets occurring in zones 1 and 2 correspond for the most part to vegetation and forest stands.
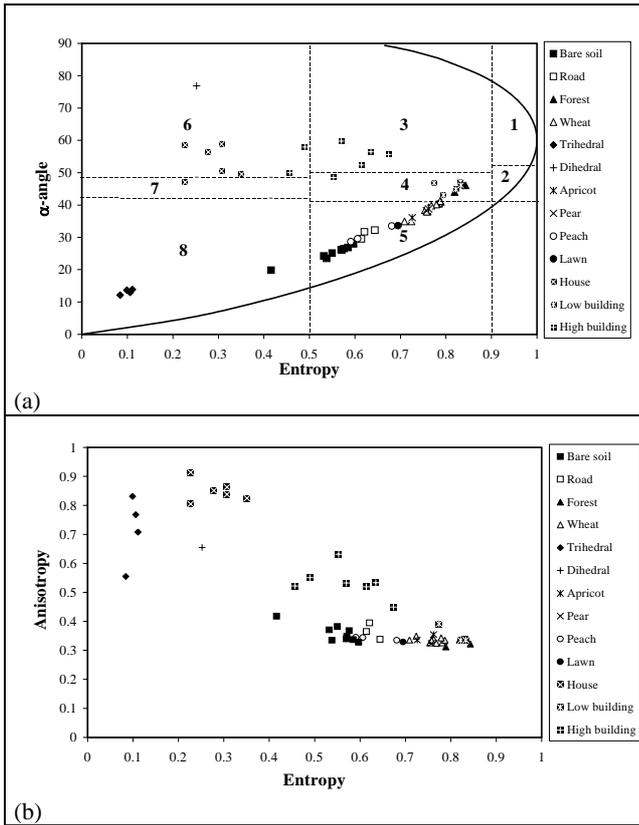
Figure 3. Entropy/$\overline{\alpha}$-angle and entropy/anisotropy scatterplots for training sites of various surface types. Each point represents the mean value of a training field.

Ferro-Famil and Pottier (2001) noted that the introduction of the anisotropy information improves the discrimination between targets. Each area in the H/$\overline{\alpha}$ plane is thus divided into two classes according to the pixels anisotropy value being greater than 0.5 or less than 0.5. For our targets, anisotropy is not a discriminating parameter at X-band. Its value is approximately the same for bare soils, roads, orchards, forest, lawn, wheat and low building (0.3<A<0.4). For the other targets (trihedral, dihedral, house and high building), the anisotropy is superior to 0.5.

The results obtained in this study are in agreement with the results obtained by Ferro-Famil and Pottier (2001). They demonstrated that in P-band, it is possible to separate the tree parcels in 3 categories; small, moderate and old trees. The results obtained in L-band indicated that different types of trees couldn't be separated precisely. In C-band no discrimination between different tree ages is possible.

This signature study demonstrates the effectiveness of polarimetric X-band for mapping specific land use classes. A decision tree model can be used to classify the scene by combining the different parameters of the radar signal (backscattering coefficients, copolarization and depolarization ratios, correlation coefficients, entropy, $\overline{\alpha}$-angle, and anisotropy). The classification rules can be easily determined from training data. The following list proposes the parameters to be used in such a classification process. By applying these parameters in order, ambiguity between classes is eliminated:

- Trihedral: VV or HV/VV or Entropy.

- Dihedral: correlation coefficient between cross and copolar or $\overline{\alpha}$-angle.
- House: depolarization ratios or Entropy or Anisotropy.
- High building: HH or HV or Anisotropy.
- Low building: HV.
- Bare soils: Entropy or $\overline{\alpha}$-angle.
- Roads: HV.
- Forest: H/$\overline{\alpha}$ plane (zone 4).
- Orchards, wheat and lawn: difficult to classify as the confusion between the classes will be large.

4.3 Relationship between surface roughness and the radar signal

For bare soils, the backscattering coefficients decrease by about 8dB in HH and VV and 10dB in HV between the two bare soil fields R4 and R5 (rms surface height of 0.85 and 0.80cm, respectively ; Figure 4). This decrease is due to the increase of both incidence angle and correlation length, and the decrease of soil moisture (cf. Table 1). The radar signal is therefore dependent on the incidence angle. This relationship is given approximately by the function $\cos^{\alpha}\theta$ (Baghdadi et al., 2000). The parameter α is dependent on the dominant scattering mechanism and sensor parameters (Shi et al., 1994). In general, for a radar frequency given, the parameter α is calculated for each surface type and each polarization. Next, the mean α is computed for each polarization by calculating the mean of α for all classes. However, for our image, only the wheat field class is present at different incidence angles. Because of this, we have used the parameter α estimated from the wheat field class data to reduce the angular dependence of the radar signal. In Table 2 the angular dependence is listed for various polarizations. The coefficient of determination R^2 is 0.95 for the HH and VV polarizations, and 0.88 for the HV polarization. Our training sites of various classes are located between incidence angles of 26° and 32°. This variation in the incidence angle could potentially cause variations in signal power of up to 1.9dB in the HH polarization, 1.6dB in the HV polarization, and 2.9dB in the VV polarization.

HH	CROSS	VV
$\cos^{7.3717}\theta$	$\cos^{6.4728}\theta$	$\cos^{11.34}\theta$

Table 2: The angular dependence of radar signal at different polarizations.

The difference in incidence angle between the two bare soil fields R4 and R5 (rms of 0.85 and 0.80cm, respectively) could cause a decrease in the radar signal of about 1.6dB in the HH polarization, 1.4dB in the HV polarization, and 2.4dB in the VV polarization. As mentioned in the literature, an increase in the surface moisture of about 5% leads to an increase of the retrodiffusion coefficient of approximately 1dB when the incidence angle is smaller than 20° (Le Toan et al., 1994). Thus, the decrease in the radar signal caused only by the decrease in soil moisture (about 14%) is approximately 3dB. The slaking crust observed in the field R5 (high correlation length comparatively to the field R4) increases the specular scattering and leads to a decrease of the radar signal of 3.4dB for the HH polarization, 5.6dB for the HV polarization, and 2.6dB for the VV polarization. It is thus possible to track the surface degradation due to the slaking process and to distinguish the freshly tilled fields (R1 to R4 as compared to R5).
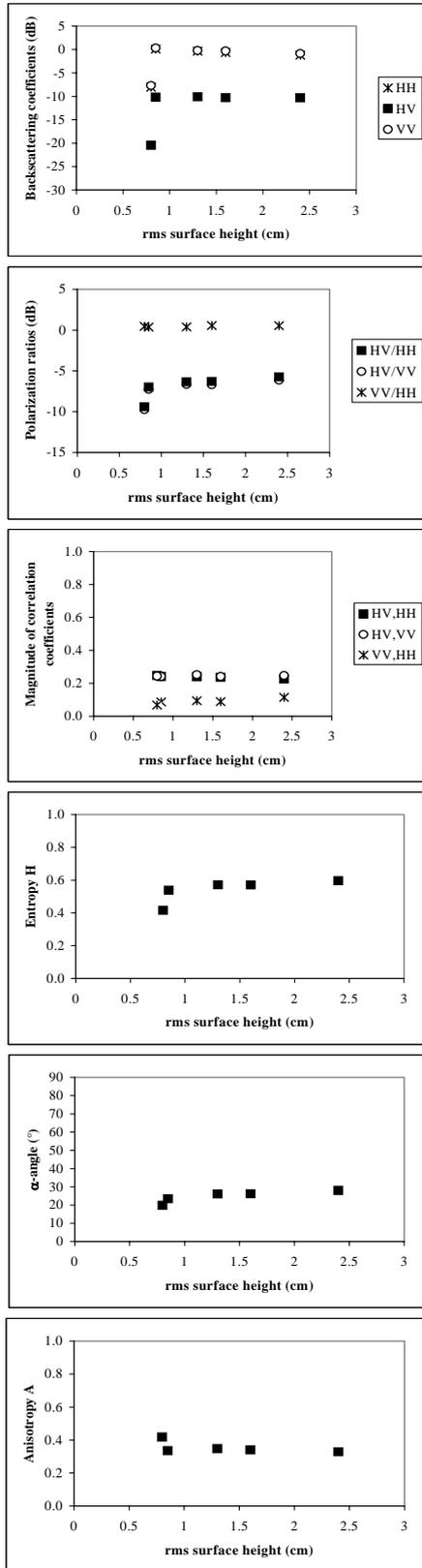
Figure 4. Variation of backscattering coefficients, copolarization and depolarization ratios, correlation coefficients and polarimetric parameters (entropy, $\overline{\alpha}$ -angle and anisotropy) as a function of rms surface height.

Our results show also that the radar signal remains virtually constant when the rms surface height increases from 0.85cm to 2.4cm (R1 to R4). We observe that the copolarization ratio reduces significantly the dependence of the radar signal on the roughness parameter. For the depolarization ratios, we observe a very weak correlation between the radar signal and the roughness parameter. As for the correlation coefficients, these were found to be much less dependent on the roughness parameter. Discrimination between the bare soils surface roughness in the H/ $\overline{\alpha}$ and H/A planes is not possible (cf. Figures 3 and 4). However, the parameters H and $\overline{\alpha}$ increase slightly with the rms surface height. As for the anisotropy, we observe the opposite behaviour, this parameter decreases with rms surface height. In conclusion, the polarimetric parameters do not provide discrimination in X-band at low incidence angle between the roughness states. However, it has been observed (Baghdadi et al., 2002) that the influence of soil roughness on radar return at C-band is higher at high incidence angles (47°) than at low incidence angles (23° and 40°). This suggests further analysis of X-band data acquired at a high incidence angle is necessary.

5. CONCLUSIONS

The potential of polarimetric SAR data at X-band has been tested with data acquired with the ONERA's RAMSES system over an area of Avignon in Southern France. The polarimetric measurements provide a more complete description of targets than is possible with a single-channel radar system. Results obtained using the backscattering coefficients and the polarimetric parameters calculated from the eigen decompostion of the coherency matrix show moderate discrimination between classes at X-band. Certain classes, wheat, lawn and orchards for example, are difficult to classify. The radar signal at X-band acquired at an incidence angle of around 26° is weakly correlated to the surface roughness over bare soils. However, it is possible to observe the surface degradation due to the slaking process and to distinguish the freshly tilled fields.

The entropy and $\overline{\alpha}$ -angle plane indicate clearly that the class signatures are grouped in five main clusters. The introduction of the anisotropy parameter does not allow discrimination between different classes whose cluster centres are in the same zone of the entropy/ $\overline{\alpha}$ plane.

These results suggests that for a more complete analysis, X-band data at a high incidence angle must be studied.

References
Baghdadi N., Bernier M., Gauthier R., and Neeson I., 2000. Evaluation of C-band SAR data for wetlands mapping. *International Journal of Remote Sensing, vol. 22, no. 1, pp. 71-88.*

Baghdadi N., King C., Bourguignon A., and Remond A., 2002. Potential of ERS and RADARSAT data for surface roughness monitoring over bare agricultural fields : application to catchments in Northern France. *International Journal of Remote Sensing, vol. 23, no. 17, pp. 3427-3442.*

Cloude S.R. and Pottier E., 1996. A review of target decomposition theorems in radar polarimetry. *IEEE Transactions on Geoscience and Remote Sensing*, vol. 34, no. 2, pp. 498-518.

Cloude S.R. and Pottier E., 1997. An entropy based classification scheme for land applications of polarimetric SAR. *IEEE Transactions on Geoscience and Remote Sensing*, vol. 35, no. 1, pp. 68-78.

Ferro-Famil L., and Pottier E., 2001. Classification de données SAR multifréquences polarimétriques. *Annals Télécommunications, vol. 56, no.9-10, pp. 510-522.*

Hajnsek I., Papathanassiou K.P., Reigber A., and Cloude S., 1999. Soil moisture estimation using polarimetric SAR data. *Proceedings IGARSS, Hamburg, 1999, vol. V, pp. 2440-2442.*

Le Toan T., Merdas M., Smacchia P., Souyris J.C., Beaudoin A., Nagid Y., and Lichtenegger J., 1994. Soil moisture monitoring using ERS-1. *2ⁿᵈ ERS-1 Symposium ESA, Hamburg, pp. 883-888.*

Scheuchl B., Caves R., Cumming I., and Staples G., 2001. Automated sea ice classification using spaceborne polarimetric SAR data. *Proceedings IGARSS, July 9-13,2001,Sydney Australia.*

Shi J., Dozier J., and Rott H., 1994. Snow Mapping in Alpine Regions with Synthetic Aperture Radar. *IEEE Transactions on Geoscience and Remote Sensing, vol. 32, no. 1, pp. 152-158.*